Surface modification of Ti-6Al-4V alloys manufactured by selective laser melting: Microstructural and tribo-mechanical characterization

Yadir Torres, Perla Sarria, Francisco José Gotor, Eliel Gutiérrez, Eduardo Peon, Ana María Beltrán, Jesús E. González

PII: S0257-8972(18)30490-0
DOI: doi:10.1016/j.surfcoat.2018.05.015
Reference: SCT 23390

To appear in: *Surface & Coatings Technology*

Received date: 19 February 2018
Revised date: 11 April 2018
Accepted date: 9 May 2018

Please cite this article as: Yadir Torres, Perla Sarria, Francisco José Gotor, Eliel Gutiérrez, Eduardo Peon, Ana María Beltrán, Jesús E. González , Surface modification of Ti-6Al-4V alloys manufactured by selective laser melting: Microstructural and tribo-mechanical characterization. The address for the corresponding author was captured as affiliation for all authors. Please check if appropriate. Sct(2017), doi:10.1016/j.surfcoat.2018.05.015

Surface modification of Ti-6Al-4V alloys manufactured by selective laser melting: Microstructural and tribo-mechanical characterization

Yadir Torres[1*], Perla Sarria[2], Francisco José Gotor[3], Eliel Gutiérrez[2], Eduardo Peon[4], Ana María Beltrán[1] and Jesús E. González[2,4]

[1]Ingeniería y Ciencia de los Materiales y del Transporte, Escuela Politécnica Superior de Sevilla, Universidad de Sevilla. Calle Virgen de África, 7, 41011 Sevilla (Spain)

[2]Group of Biomechanic, Department of Mechanical Engineering Technology, Technological University of Havana "José Antonio Echeverría", Dirección Calle 114, # 11901, e/ Ciclovía y Rotonda, Marianao, Cujae. La Habana. Cuba.

[3]Materials Science Institute of Seville (CSIC-US), Instituto de Ciencia de Materiales de Sevilla (CSIC-Univ. Sevilla), Avda. Américo Vespucio 49, 41092-Sevilla, Spain

[4]Department of Ceramic and Metallic Biomaterials, Biomaterials Center, University of Havana, Avenida Universidad s/n entre G y Ronda, Vedado, apartado postal 6323. Plaza de la Revolución. La Habana. Cuba

*Departamento de Ingeniería y Ciencia de los Materiales y del Transporte, Escuela Politécnica Superior de Sevilla, Universidad de Sevilla. Calle Virgen de África, 7, 41011 Sevilla (Spain) ytorres@us.es; Telephone: +34 954482279

Abstract.

Medical grade of both titanium (Ti) and Ti6Al4V alloy are recognized as the metallic biomaterials with the better outcomes for clinical repair of bone tissue thanks to their suitable mechanical properties and corrosion resistance. However, those Ti advantages are not enough to avoid failure risks of bone implants; between 5 and 10% of Ti implants fail due to a deficient osseointegration, within 5 years of post-implantation. Most of these failures indicate the necessity of getting a better biomechanical-biofunctional balance. Microstructural and tribo-mechanical characterizations were performed on Ti6Al4V samples obtained by selective laser melting and subjected to different surface treatments (thermal stress relief, acid etching,

chemical treatment and thermo-chemical treatment). Scanning electron microscopy and X-ray diffraction were used for detailed characterization of the elemental composition, phase analysis and surface morphology. Micro-hardness and scratch tests were employed to evaluate the tribo-mechanical properties, which were improved after consecutive surface treatments. Protuberances with spherical morphology, as a remainder of the original powder, were present on the surface. The resulting modified surfaces were constituted by rutile (major phase) and anatase (minor phase). Submicro-nano-topographies were obtained after the chemical and thermochemical treatments.

Keywords: Selective Laser Melting, surface modification, titanium alloys, tribo-mechanical behavior, biomaterials

1. Introduction

The tissues of the musculoskeletal system, especially bones, suffer significant degradation, mostly associated with life habits, diseases and aging. As world population becomes increasingly aged, especially in the more developed regions, musculoskeletal disorders are more frequent and the high cost associated with surgical implant operations induces a high pressure on the public health systems. Moreover, as a result of strong physical activity, genetics or traumas (typically accidents), there is also an increasing need for prostheses for younger patients and then able to withstand important stress levels over longer periods. Therefore, it exists a real demand for long-lasting implants with a good balance between biomechanical and biofunctional properties and with a competitive production cost.

Commercially pure titanium (cp-Ti) and Ti-based alloys, especially Ti6Al4V that accounts for more than 50% of total Ti usage, are recognized as excellent metallic biomaterials for bone tissue replacement due to a unique combination of properties. They have excellent biocompatibility, high specific strength, high-fatigue performance and good corrosion resistance [1,2]. Despite these good properties, the reliability of Ti-based implants must be improved to minimize some biomechanical and biofunctional failures. On the one hand, biomechanical failures are mainly due to Young's modulus mismatch between the implant and the bone tissue that creates stress-shielding (inhomogeneous stress transfer between the implant and the bone) [3], and may be the cause of bone resorption, poor osseointegration and refracturing [4]. Moreover, an excessive loading applied to the implant or the improper design can also lead to fatigue failure [5]. On the other hand, biofunctional failures are related to the deterioration of the implant-bone interface caused by excessive micromotion [6], resulting in fibrous tissue encapsulation and implant loosening. Microbial contamination [7] during trauma,

surgery or via remote infections, which can manifest in the early stages of recovery or even after a number of months postoperatively, is another major cause that can lead to the failure of implants.

For proper osseointegration of implants, which positively affects the clinical success and shorten the healing time, it is necessary to stimulate the adhesion, proliferation and differentiation of osteogenic cells at the implant-bone interface. This can be achieved by modifying different surface properties, such as the topography (roughness, porosity, compactness, morphology), the surface energy and the chemical and phase compositions [8]. This can be done by means of different surface treatments, including abrasive blasting [9,10], chemical etching [10-12], electrochemical process [13,14], thermal treatment [15,16] and laser treatment [17,18], among others. Frequently, different surface treatments are combined in a particular process sequence to reach the desired microstructure and physicochemical properties [10,15-17]. It has been proven that most of these treatments modify simultaneously the topography and the chemical composition of the biomaterial surface [19,20].

The deposition of bioactive coatings on the surface of the implant, e.g., synthetic hydroxyapatite [21] or bioactive glass [22], using different methods, such as plasma spraying [23], electrodeposition [21], biomimetic [24] and sol-gel [25], has also been widely studied. *In vitro* and *in vivo* evaluation of these coatings is necessary due to long-term adhesion and degradation problems [26]. The immobilization of biomolecules on the implant surface [27], including the bone growth factors [28], and the implantation of bioactive trace elements [29] have also been proposed to promote the cell response.

Ti-based implants and prostheses can be manufactured using different methods and procedures, such as conventional and computer numerical control (CNC) machining [30] (generally from forged or casted blanks), forging, rolling [31], powder metallurgy [32-35], injection molding (IM) [36], etc. Metal additive manufacturing (AM) processes are acquiring increasing interest because they are able to produce complex parts. In this technology, the final geometry is obtained from a process of melting and solidification of metallic powders layer upon layer, following a digital computer-aided design (CAD) 3D model. Various AM methods differ on feedstock material (powder, wire), energy source (laser beam, electron beam, plasma beam) and manufacture process (melting, sintering, deposition) [37-39]. AM methods allow high design flexibility, reduced processing time, waste and costs of the manufacture of custom-shaped parts that cannot be made by conventional routes. Moreover, they avoid the problems found in conventional manufacturing routes, related to the low thermal conductivity and high reactivity of Ti-based materials.

In selective laser melting (SLM) method [40-43], a high intensity laser beam is focused and scanned according to the design model onto a powder layer with a defined thickness (fed from a supply container), in such a way that a selected area is melted, fused to the previous layer and rapidly solidified because of an extremely short thermal cycle. The process is repeated until all the layers according to the 3D model have been transferred to the building platform. Furthermore, the density, the microstructure, the surface characteristics and the mechanical properties of the obtained parts can be adjusted by modifying the processing parameters during SLM [42,44]. Although SLM produces intrinsically rough surfaces, its topography or the chemical surface composition obtained may not be ideal for promoting osseointegration. For these reasons, suitable surface modification treatments may be required [45,46]. In this context, the aim of this

work was to investigate the effects of combining the intrinsic topography of Ti6Al4V samples manufactured by SLM with submicro-nano-topographies obtained through different chemical and thermochemical surface treatments.

2. Materials and Methods

2.1. Processing of samples

Commercial Ti6Al4V alloy powder (grade V supplied by SLM Solutions GmbH) was employed as raw material in SLM process. The Ti6Al4V powder had a spherical morphology and an equivalent diameter of 31±12 μm, with minimum and maximum dimensions of 10 and 65 μm, respectively. Plates 20x14x1 mm in size and cylindrical samples 8 mm in diameter and 11.7 mm in height were manufactured in a SLM 250^{HL} machine (Solutions GmbH, Germany) in a continuous mode. A laser power of 200 W, exposure time of 3 s and layer thickness of 50 μm were used. Samples were designed with Inventor Professional 3D CAD software (Autodesk Inc, California, USA).

Five samples with different surface treatments were prepared and studied in this work. Prior to each surface modification, the surfaces of the samples were successively ultrasonically cleaned in acetone (15 min), alcohol (20 min) and distilled water (20 min). All the samples were manufactured by SLM. However, samples B to E were also treated. Sample B was subjected to a stress relief heat treatment consisting of 10 min at 750 °C in static air (heat treatment, heating rate of 15 ºC/min and furnace cooling) in a KBF1200 furnace (Koyo Thermo Systems Co., Ltd, Japan). Sample C was etched in an acidic solution (100 ml of HCl, 18 wt %, and 100 ml of H_2SO_4, 48 wt %) and then complete immersion for 30 min at room temperature. Sample D was acid etched as sample C but followed by a chemically treatment in a solution containing 8.8 M H_2O_2 and 0.1 M HCl at 80 ºC for 30 min. Finally, sample E was treated as sample D but later

heat-treated at 400 ºC for 1 h in static air (thermochemical treatment, heating and cooling rate of 10 ºC/min). Samples description is summarized in Table 1.

Table 1: Sample description.

SAMPLE	TREATMENT
A	Reference sample, SLM
B	Sample A + Annealing 750 ºC, 10 min
C	Sample B + Acid etched
D	Sample C + Chemical treatment
E	Sample D + Thermochemical treatment 400 ºC, 1 h

2.2. Characterization of samples

The surface morphology of different samples was characterized by scanning electron microscopy (SEM) using a Hitachi S-4800 SEM-Field Emission Gun microscope in secondary electron mode. The protuberance size on the five studied surfaces was compared employing Statgraphics Centurion XV software and differences were evaluated using a multiple range comparison with a multiple range test. In this test, a confidence level of 95% ($p < 0.05$) was considered as statistically significant. The elemental composition was determined by energy dispersive X-ray spectroscopy (XEDS) with a detector (Quantax-EDS, Bruker Corporation) coupled to the SEM microscope.

The phase identification was performed by X-ray diffraction (XRD) using a PANalytical X'Pert Pro instrument equipped with a θ/θ goniometer, using Cu Kα radiation (40 kV, 40 mA), a secondary K_β filter and an X'Celerator detector. The diffraction patterns were scanned from 20º to 140º (2θ) in step-scan mode with a step

size of 0.05º and a counting time of 300 s/step. The phases detected were elucidated using the PDF-4+ database from the International Centre for Diffraction Data (ICDD).

Micro-hardness measurements were performed using a micro-Vickers indenter Shimadzu (model HMV-G) at different loads (10, 25 and 100 g), according to ASTM E384–05a [47]. Additionally, after removing the modified surfaces by grinding and polishing processes, the micro-hardness (HV0.1) of the bulk material was evaluated. Ten measurements were made for each sample and load. Furthermore, the scratch tests were carried out in a MICROTEST commercial device (MTR3/50-50/NI) using a Rockwell diamond tip with a diameter of 200 µm and constant load of 20 N at a rate of 0.5 mm/min for 5 mm length (ASTM C1624-05 [49]). The normal load was continuously recorded during scratching and sliding contact response was given in terms of scratch penetration-load curves. The real plastic deformation (deformation after scratching) and the elastic recovery (difference in depth between the scratch and post-scan curves) were measured for each sample. At least three roughness profiles and scratch tests of each samples were performed. Finally, the micro-scratch scars were examined along the whole scratch length to discern the contact damage feature. The roughness parameters were obtained at a speed of 0.5 mm/min and without applied load. Different roughness parameters were determined: the arithmetic average of the absolute values of all points of the profile (*Ra*), the root mean square of the values of all points of the profile *(Rq),* the maximum peak-to-valley height of the entire measurement trace *(Ry*) and the arithmetic average of the maximum peak-to-valley height of the roughness values of five consecutive sampling sections over the filtered profile *(Rz).*

3. Results and Discussion

SEM images of the surface of the Ti6Al4V samples showed protuberances with almost spherical morphology (Figure 1), which in fact correspond to a remnant of partially molten particles of the powder alloy as proved by a size distribution similar to the starting powder. The number of particles adhered to the surface was not significantly affected by the different surface treatments. In general, statistically no significant differences were found among the protuberances sizes (Figure 2). Only, a small increase in size was observed in D and E surfaces, which could be related to the formation of an outer oxide layer. In addition, the size of the protuberances in sample C showed statistical significant differences compared to B, D and E samples. Figure 3 shows that in these samples, many protuberances are cracked, and when they are pulled out, the different appearance between the attacked surface and the support underneath is clearly observed.

Figure 4 displays the five studied surfaces at higher magnification. The existence of an oxide layer (as it will be confirmed by XRD) was observed, except for sample A, without any surface treatment. In sample B, an oxide layer with a porous structure (pores in sub-micrometric scale) was evidenced. This layer was composed of sub-micrometric and nano-metric platelike particles and it was the result of the temperature used during the thermal treatment. This high temperature treatment was employed in order to produce a stress relief in samples, since the high thermal gradients existing during the SLM process can produce a high level of residual stresses. The acidic etching (sample C) also produced a thin and sub-micro-porous oxide layer. However, when the sample was chemically treated in a H_2O_2 solution after the acidic etching (sample D), a submicro-nano-porous surface with even smaller particles and a more rounded morphology was obtained. This specific morphology can be positive for osseointegration of implantable devices. The subsequent thermochemical treatment at

400 ºC for 1h (sample E) did not significantly modify the surface porosity and pore size in comparison to surface D. In addition, on the surface E, a platelike structure with thickness in the nanometer scale was predominantly observed. Some dense particles were also noticed (Figure 4, sample E). Tissue integration to the metallic implants and its long-term stability result from the interactions between its surface and the surrounding biological environment at the cellular and molecular level [50,51] and it has been reported that nanostructured surfaces on metal implants enhanced the osteogenic activity [52].

To obtain information on the nature of the oxide phases present on the surface of the Ti6Al4V alloy, XRD patterns of the five surfaces studied were collected (Figure 5). The XRD pattern of the as-manufactured sample (sample A), without any subsequent surface treatment, did not reveal the formation of any oxide phase on its surface since no characteristic peaks of oxides phases were observed. The XRD diagram of sample A matches the ICDD reference pattern 44-1294 corresponding to the hcp structure characteristic of the α-phase. The absence of β-phase peaks in the XRD pattern of this sample must be an indicative of the presence of α′ martensite also with hcp structure [53]. The metallographic analysis of the bulk confirmed the existence of both α- and α′-phases (see support information, Figure S1). The broadening of the reflections corresponding to the Ti6Al4V alloy was reduced in sample B due to the stress relief heat treatment. In this sample, the XRD peaks of the rutile phase (ICDD reference pattern 21-1276) were also clearly detected together with a small amount of anatase (ICDD reference pattern 21-1272). Similar XRD patterns were observed for the other samples (samples C and D), in which a major rutile phase and a minor anatase phase were formed on the surface too. Small-angle XRD measurements showed similar patterns to those in Figure 5, with the XRD peaks of the Ti6Al4V alloy phase clearly

visible. This suggests that the oxide layer was really thin. These patterns did not reveal the formation of TiO_2 amorphous phase.

Semi-quantitative XEDS-SEM analyses were performed on the surface of the different samples to detect any segregation in the Ti6Al4V alloy due to the surface treatments. The presence of Ti, Al and V was observed in all the samples, but O was only detected in the treated samples, as it is shown in Figure 6, in which, as an example, XEDS spectra of samples A and D are compared. The XEDS spectra of the other samples were similar to that of sample D. Table 2 lists the calculated chemical compositions by semi-quantitative XEDS-SEM analysis. Oxygen content was not determined because XEDS is not appropriate for the quantification of light elements. The results in Table 2 revealed that the surface treatments did not induce significant variations in the Ti, Al and V concentrations at the surface. Only a slight enrichment in Al was appreciated.

Table 2. Chemical composition of the surfaces of Ti6Al4V samples determined by semi-quantitative XEDS-SEM analysis.

Samples	**Al [wt.%]**	**Ti [wt.%]**	**V [wt.%]**	**Ratio**	
				Ti/Al	Ti/V
A	4.8±0.3	92.3±0.6	2.9±0.4	19.3	31.7
B	6.9±0.8	90.7±0.8	2.5±0.6	13.2	36.7
C	7.1±0.2	90.1±0.2	2.8±0.3	12.7	32.6
D	7.7±0.3	89.9±0.3	2.4±0.1	11.6	38.1
E	6.2±0.7	91.2±0.5	2.5±0.1	14.6	36.0

Table 3 shows the Vickers micro-hardness values obtained on the surface of the samples and after removal of the oxide layers (bulk measurement). A large dispersion was observed in the surface micro-hardness, especially for the treated samples, that was

attributed to the fact that the measurements were performed over the protuberances. It was experimentally observed that the micro-hardness of the smaller protuberances was greater than that of the larger ones. Moreover, protuberances that appeared to be more partially molten also presented a higher micro-hardness. On the other hand, if the HV0.1 values are compared, which are less influenced by the size of protuberances, a higher micro-hardness was observed in superficially treated samples because of the formation of the oxide layer. However, the micro-hardness after removal of the oxide layer was slightly lower in sample subjected to the stress relief annealing treatment.

Table 3. Vickers micro-hardness of the surfaces of samples and after removal the outermost layer (bulk measurement).

Samples	**Surface protuberances**		**Bulk**
	HV0.025	HV0.1	HV0.1
A	530 ± 22	384 ± 71	496 ± 58
B	361 ± 173	600 ± 49	440 ± 24
C	388 ± 171	519 ± 121	
D	499 ± 81	655 ± 58	
E	663 ± 138	644 ± 89	

The surface roughness profile and the associated parameters for the different Ti6Al4V samples are presented in Figure 7 and Table 4, respectively. Sample C subjected to an acid etching presented the lowest surface roughness, while sample D with acid etching and chemical treatment with H_2O_2 had the highest surface roughness. In this case, the increasing roughness was attributed to the formation of the porous surface and to the oxide layer thickness (Figure 4). In general, the surface roughness after performing the scratch test, measured inside the micro-scratch scars, was smaller, which was associated

with plastic deformation phenomena. However, in sample E, the surface roughness increased, probably due to a higher amount of debris and chipping that remained inside the scar.

Table 4. Surface roughness parameters of different Ti6Al4V samples.
Note: The relative error is lower than 1 and 2 % before and after, respectively.

Parameters	**A**		**B**		**C**		**D**		**E**	
	Before	After	Before	After	Before	After	Before	After	Before	After
$\mathbf{R_a}$ (μm)	8.0	6.2	9.9	6.2	6.4	5.6	10.0	7.7	8.0	14.7
$\mathbf{R_q}$ (μm)	10.9	7.7	11.7	7.7	7.8	7.4	13.1	9.3	10.1	17.0
Ry (μm)	52.9	40.4	50.9	36.1	42.1	35.9	60.3	38.8	49.0	66.0
$\mathbf{R_z}$ (μm)	48.3	28.9	36.5	16.3	29.4	18.7	48.1	38.1	47.1	53.0

The scratch test results for the Ti6Al4V samples are presented in Figure 8, where the difference between the in-situ penetration depth and the real plastic deformation associated with the scratch tests (elastic recovery) is illustrated. The scratch tracks are shown in Figure 9. Table 5 presents the average values for the penetration depth, the plastic deformation and the elastic recovery obtained from Figure 8 for the different Ti6Al4V samples. Note that the surface treatments have a clear effect on these values. For example, the elastic recovery was reduced in sample B if compared to sample A due to the stress relief treatment. It is also observed that the degree of elastic recovery decreases continually as the successive surface treatments are performed as a result of an increased thickness and hardness of the surface oxide layer. The behavior of the titanium bulk (pseudo-plastic material) is clearly different from that obtained on the surface of the treated samples.

Table 5. Average penetration depth (Pd), average plastic deformation (Pl) and average elastic recovery (Er) obtained from the scratch tests (constant load, 20N during 5mm at 0.5 mm/min).

	Bulk	**A**	**B**	**C**	**D**	**E**
Pd (μm)	215.8 ± 18.5	47.4 ± 4.8	67.4 ± 3.5	38.2 ± 8.7	12.0 ± 8.9	46.8 ± 23.5
Pl (μm)	21.1 ± 3.4	8.0 ± 9.7	40.6 ± 7.7	15.3 ± 7.4	4.6 ± 9.3	42.8 ± 17.0
Er (μm)	194.7 ± 18.8	39.4 ± 10.8	26.8 ± 8.5	22.9 ± 11.4	16.6 ± 12.9	4.0 ± 29.0

Furthermore, during the scratch tests at 20 N all the surfaces showed failures (Figure 8). At this load, on the surfaces A and C was detected plastic deformation, while on the surfaces B and C some micro-cracks were observed. The plastic deformation of these surfaces was linked to the lower micro-hardness of the substrate (Table 3). In addition, the surfaces D and E presented micro-cracks and recovery spallation (adhesive failure). This failure mode is produced by the elastic recovery of the scratch track and depends on the plastic deformation in the substrate and cracking of the coating [56].

In summary, no representative changes of the micro-topography surface were observed after the performed treatment, although sub-micro and even nano-features could be appreciated (Figure 4). The analyses of the treated surfaces by different routes showed: (1) statistically significant increase in protuberances size of samples B, D and E compared to the reference sample A. It could be related to a higher thickness of the oxide layers because of a greater degree of oxidation of the elements of the substrate (Ti, Al and V) during the chemical or thermochemical processes. Additionally, an increase of the oxygen diffusion coefficient was produced on thermochemical treated surfaces (samples B and E), that also influenced the oxide layer thicknesses. (2) Treatment C (acid etching) caused a decrease of the protuberances size. (3) Titanium oxides (anatase and rutile) were detected on all the surfaces. In fact, the presence of Ti-oxides layers, as micro- and nano-texture, have been extensively studied since it has

been related to the stimulation of the osseointegration of titanium implants [57]. (4) The tribo-mechanical behavior was related to the role of the oxide layer, being scratch resistance and micro-hardness higher while elastic recovery lower, compared to the bulk reference.

4. Conclusions

In this work, Ti6Al4V alloys were manufactured by SLM and subsequently subjected to surface modification by different chemical and/or thermo-chemical treatments. All the surfaces subjected to these treatments presented the formation of a stable titanium oxide layer, composed of major rutile and minor anatase, which can be beneficial to enhance the bioactivity of the surface. In addition, all the samples exhibited a rough surface, on which partially molten particles coming from the starting powder were adhered. These particles formed protuberances on the surfaces with an almost spherical morphology. The protuberance size on the surfaces D (with acid etching plus chemical oxidation in an aqueous solution of peroxide) and E (surface D plus thermochemical treatment) were higher than the observed on the rest of the surfaces due to the formation of an outer oxide layer.

It was also demonstrated that it is possible to modify the topography of the Ti6Al4V alloy obtained by SLM at the nano-scale without affecting its morphology and topography at the micro-scale. The surfaces with chemical oxidation and chemical oxidation plus thermochemical treatment exhibited multiscale topographies (micro submicro and nano-roughness). These surfaces were fully covered by submicro- and nano-pores. Besides, a higher microhardness and lower elastic recovery after the scratch tests were observed in samples superficially modified due to the presence of the oxide layer scale.

Acknowledgments

This work was supported by the Junta de Andalucía-FEDER (Spain) through the Project Ref. P12-TEP-1401 and by the Spanish Ministry of Economy and Competitiveness under the Grant No. MAT2015-71284-P.

References

1. M. Niinomi, Mechanical biocompatibilities of titanium alloys for biomedical applications, Journal of the Mechanical Behavior of Biomedical Materials 1 (2008) 30-42. DOI: 10.1016/j.jmbbm.2007.07.001

2. F. A. Shah, M. Trobos, P. Thomsen, A. Palmquist, Commercially pure titanium (cp-Ti) versus titanium alloy (Ti6Al4V) materials as bone anchored implants — Is one truly better than the other?, Materials Science and Engineering C 62 (2016) 960–966. DOI: 10.1016/j.msec.2016.01.032

3. M. Niinomi, M. Nakai, Titanium-based biomaterials for preventing stress shielding between implant devices and bone, International Journal of Biomaterials, 2011 (2011) 836587. DOI: dx.doi.org/10.1155/2011/836587

4. A. Gefen, Computational simulations of stress shielding and bone resorption around existing and computer-designed orthopaedic screws, Medical & Biological Engineering & Computing 40 (2002) 311–322.

5. M. Karl, J. R. Kelly, Influence of loading frequency on implant failure under cyclic fatigue conditions, Dental Materials 25 (2009) 1426–1432. DOI: 10.1016/j.dental.2009.06.015

6. R. M. Wazen, J. A. Currey, H. Guo, J. B. Brunski, J. A. Helms, A. Nanci, Micromotion-induced strain fields influence early stages of repair at bone–implant interfaces, Acta Biomaterialia 9 (2013) 6663–6674. DOI: 10.1016/j.actbio.2013.01.014

7. S. Qian, Y. Qiao, X. Liu, Selective biofunctional modification of titanium implants for osteogenic and antibacterial applications, Journal of Materials Chemistry B 2 (2014) 7475–7487. DOI: 10.1039/C4TB00973H

8. L. Le Guëhennec, A. Soueidan, P. Layrolle, Y. Amouriq, Surface treatments of titanium dental implants for rapid osseointegration, Dental Materials 23 (2007) 844–854. DOI: 10.1016/j.dental.2006.06.025

9. K. Anselme, P. Linez, M. Bigerelle, D. Le Maguer, A. Le Maguer, P. Hardouin, H. F. Hildebrand, A. Iost, J.M. Leroy, The relative influence of the topography and chemistry of TiAl6V4 surfaces on osteoblastic cell behavior, Biomaterials 21 (2000) 1567–1577.

10. J. I. Rosales-Leal, M. A. Rodríguez-Valverdeb, G. Mazzaglia, P. J. Ramón-Torregrosa, L. Díaz-Rodríguez, O. García-Martínez, M. Vallecillo-Capilla, C. Ruiz, M. A. Cabrerizo-Vílchez, Effect of roughness, wettability and morphology of engineered titanium surfaces on osteoblast-like cell adhesion, Colloids and Surfaces A: Physicochemical and Engineering Aspects 365 (2010) 222–229. DOI: 10.1016/j.colsurfa.2009.12.017

11. X. X. Wang, S. Hayakawa, K. Tsuru, A. Osaka, Bioactive titania gel layers formed by chemical treatment of Ti substrate with a H2O2/HCl solution, Biomaterials 23 (5) (2002) 1353–1357.

12. C. Zhao, K. Liang, J. Tan, Z. Xiang, H. Fan, X. Zhang, Bioactivity of porous titanium with hydrogen peroxide solution with or without tantalum chloride treatment at

a low temperature, Biomedical Materials 8 (2013) 025006. DOI: 10.1088/1748-6041/8/2/025006

13. X. Zhu, J. Chen, L. Scheideler, R. Reichl, J. Geis-Gerstorfera, Effects of topography and composition of titanium surface oxides on osteoblast responses, Biomaterials 25 (2004) 4087–4103. DOI: 10.1016/j.biomaterials.2003.11.011

14. A. Krząkała, A. Kazek-Kęsik, W. Simka, Application of plasma electrolytic oxidation to bioactive surface formation on titanium and its alloys, RSC Advances 3 (2013) 19725-19743. DOI: 10.1039/C3RA43465F

15. B. H. Lee, Y. D. Kim, J. H. Shin, K. H. Lee, Surface modification by alkali and heat treatments in titanium alloys, Journal of Biomedical Materials Research 61 (3) (2002) 466–473. DOI: 10.1002/jbm.10190

16. S. Ferraris, S. Spriano, G. Pan, A. Venturello, C.L.Bianchi, R. Chiesa, M. G. Faga, G. Maina, E. Vernè, Surface modification of Ti–6Al–4V alloy for biomineralization and specific biological response: Part I, inorganic modification, Journal of Materials Science: Materials in Medicine 22 (2011) 533–545. DOI: 10.1007/s10856-011-4246-2

17. F. Parsikia, P. Amini, S. Asgari, The effect of multiple surface treatments on biological properties of Ti-6Al-4V alloy, Metallurgical and Materials Transactions A 45 (10) (2014) 4588–4593.

18. Y. S. Tian, C. Z. Chen, S. T. Li, Q.H. Huo, Research progress on laser surface modification of titanium alloys, Applied Surface Science 242 (2005) 177–184. DOI: 10.1016/j.apsusc.2004.08.011

19. T. Kokubo, F. Miyaji, H. M. Kim, T. Nakamura, Spontaneous formation of bonelike apatite layer on chemically treated titanium metals, Journal of the American Ceramic Society 79 (4) (1996) 1127–1129. DOI: 10.1111/j.1151-2916.1996.tb08561.x

20. J. M. Wu, S. Hayakawa, K. Tsuru, A. Osaka, Low-temperature preparation of anatase and rutile layers on titanium substrates and their ability to induce in vitro apatite deposition, Journal of the American Ceramic Society 87 (9) (2004) 1635–1642. DOI: 10.1111/j.1551-2916.2004.01635.x

21. A. Kar, K. S. Raja, M. Misra, Electrodeposition of hydroxyapatite onto nanotubular TiO2 for implant applications, Surface and Coatings Technology 201 (2006) 3723–3731. DOI: 10.1016/j.surfcoat.2006.09.008

22. J. Pavón, E. Jiménez-Piqué, M. Anglada, S. López-Esteban, E. Saiz, A. P. Tomsia, Stress–corrosion cracking by indentation techniques of a glass coating on Ti6Al4V for biomedical applications, Journal of the European Ceramic Society 26 (2006) 1159–1169. DOI: 10.1016/j.jeurceramsoc.2005.01.045

23. X. Liu, Ray W. Y. Poon, S. C. H. Kwok, P. K. Chu, C. Ding, Plasma surface modification of titanium for hard tissue replacements, Surface and Coatings Technology 186 (2004) 227–233. DOI: 10.1016/j.surfcoat.2004.02.045

24. Y. Li, W. Yang, X. Li, X. Zhang, C. Wang, X. Meng, Y. Pei, X. Fan, P. Lan, C. Wang, X. Li, Z. Guo, Improving osteointegration and osteogenesis of three-dimensional porous Ti6Al4V scaffolds by polydopamine-assisted biomimetic hydroxyapatite coating, ACS Applied Materials and Interfaces 7 (2015) 5715−5724. DOI: 10.1021/acsami.5b00331

25. C. Wu, Y. Ramaswamy, D. Gale, W. Yang, K. Xiao, L. Zhang, Y. Yin, H. Zreiqat, Novel sphene coatings on Ti–6Al–4V for orthopedic implants using sol–gel method, Acta Biomaterialia 4 (2008) 569–576. DOI: 10.1016/j.actbio.2007.11.005

26. E. R. U. Edreira, J. G. C. Wolke, A. A. Aldosari, S. S. Al-Johany, S. Anil, J. A. Jansen, J. J. J. P. van den Beucken, Effects of calcium phosphate composition in sputter coatings on in vitro and in vivo performance, Journal of Biomedical Materials Research A, 103 (2015) 300–310. DOI: 10.1002/jbm.a.35173

27. J. Michael, R. Beutner, U. Hempel, D. Scharnweber, H. Worch, B. Schwenzer, Surface modification of titanium-based alloys with bioactive molecules using electrochemically fixed nucleic acids, Journal of Biomedical Materials Research Part B: Applied Biomaterials 80B (1) (2007) 146–155. DOI: 10.1002/jbm.b.30579

28. H. Zhang, M. Ahmad, G. Gronowicz, Effects of transforming growth factor-beta 1 (TGF-β1) on in vitro mineralization of human osteoblasts on implant materials, Biomaterials 24 (2003) 2013–2020.

29. T. R. Rautray, R. Narayanan, T. Y. Kwon, K. H. Kim, Surface modification of titanium and titanium alloys by ion implantation, Journal of Biomedical Materials Research Part B: Applied Biomaterials 93B (2) (2010) 581–591. DOI: 10.1002/jbm.b.31596

30. M. V. Ribeiro, M. R. V. Moreira, J. R. Ferreira, Optimization of titanium alloy (6Al-4V) machining, Journal of Materials Processing Technology 143–144 (2003) 458-463. DOI: 10.1016/S0924-0136(03)00457-6

31. Y. Okazaki, On the effects of hot forging and hot rolling on the microstructural development and mechanical response of a biocompatible Ti alloy, Materials 5 (2012) 1439–1461. DOI: 10.3390/ma5081439

32. Y. Torres, S. Lascano, J. Bris, J. Pavón, J. A. Rodriguez, Development of porous titanium for biomedical applications: A comparison between loose sintering and space-holder techniques, Materials Science and Engineering C 37 (2014) 148–155. DOI: /10.1016/j.msec.2013.11.036

33. Y. Torres, P. Trueba, J. Pavón, I. Montealegre, J. A. Rodriguez-Ortiz, Designing, processing and characterisation of titanium cylinders with graded porosity: An alternative to stress-shielding solutions, Materials and Design 63 (2014) 316–324. DOI: 10.1016/j.matdes.2014.06.012

34. Y. Torres, P. Trueba, J. J. Pavón, E. Chicardi, P. Kamm, F. García-Moreno, J. A. Rodriguez-Ortiz, Design, processing and characterization of titanium with radial graded porosity for bone implants, Materials and Design 110 (2016) 179–187. DOI: 10.1016/j.matdes.2016.07.135

35. B. Q. Li, C. Y. Wang, X. Lu, Effect of pore structure on the compressive property of porous Ti produced by powder metallurgy technique, Materials and Design, 50 (2013) 613–619. DOI: 10.1016/j.matdes.2013.02.082

36. O. M. Ferri, T. Ebel, R. Bormann, High cycle fatigue behaviour of Ti–6Al–4V fabricated by metal injection moulding technology, Materials Science and Engineering A 504 (2009) 107–113. DOI: 10.1016/j.msea.2008.10.039

37. A. T. Sidambe, Biocompatibility of advanced manufactured titanium implants—A Review, Materials 7 (2014) 8168-8188. DOI: 10.3390/ma7128168

38. S. F. S. Shirazi, S. Gharehkhani, M. Mehrali, H. Yarmand, H. S. C. Metselaar, N. A. Kadri, N. A. A. Osman, A review on powder-based additive manufacturing for tissue engineering: selective laser sintering and inkjet 3D printing, Science and Technology of Advanced Materials 16 (2015) 033502. DOI: 10.1088/1468-6996/16/3/033502

39. M. Qian, W. Xu, M. Brandt, H. P. Tang, Additive manufacturing and postprocessing of Ti-6Al-4V for superior mechanical properties, MRS Bulletin 41 (10) (2016) 775–784. DOI: 10.1557/mrs.2016.2

40. D. A. Hollander, M. von Walter, T. Wirtz, R. Sellei, B. Schmidt-Rohlfing, O. Paar, H. J. Erli, Structural, mechanical and in vitro characterization of individually structured Ti–6Al–4V produced by direct laser forming, Biomaterials 27 (2006) 955–963. DOI: 10.1016/j.biomaterials.2005.07.041

41. L. E. Murr, S. M. Gaytan, D. A. Ramirez, E. Martinez, J. Hernandez, K. N. Amato, P. W. Shindo, F. R. Medina, Metal fabrication by additive manufacturing using laser and electron beam melting technologies, Journal of Materials Science and Technology 28 (1) (2012) 1–14. DOI: 10.1016/S1005-0302(12)60016-4

42. H. Attar, M. Calin, L. C. Zhang, S. Scudino, J.Eckert, Manufacture by selective laser melting and mechanical behavior of commercially pure titanium, Materials Science and Engineering A 593 (2014) 170–177. DOI: 10.1016/j.msea.2013.11.038

43. H. Gong, K. Rafi, H. Gu, G. D. J. Ram, T. Starr, B. Stucker, Influence of defects on mechanical properties of Ti–6Al–4 V components produced by selective laser melting and electron beam melting, Materials and Design 86 (2015) 545–554. DOI: 10.1016/j.matdes.2015.07.147

44. S. Zhang, Q. Wei, L. Cheng, S. Li, Y. Shi, Effects of scan line spacing on pore characteristics and mechanical properties of porous Ti6Al4V implants fabricated by selective laser melting, Materials and Design 63 (2014) 185–193. DOI: 10.1016/j.matdes.2014.05.021

45. D. K. Pattanayaka, A. Fukuda, T. Matsushita, M. Takemoto, S. Fujibayashi, K. Sasaki, N. Nishida, T. Nakamura, T. Kokubo, Bioactive Ti metal analogous to human cancellous bone: Fabrication by selective laser melting and chemical treatments, Acta Biomaterialia 7 (2011) 1398–1406. DOI: 10.1016/j.actbio.2010.09.034

46. G. Pyka, G. Kerckhofs, I. Papantoniou, M. Speirs, J. Schrooten, M. Wevers, Surface roughness and morphology customization of additive manufactured open porous Ti6Al4V structures, Materials 6 (2013) 4737–4757. DOI: 10.3390/ma6104737

47. ASTM E384-05a, Standard test method for microindentation hardness of materials, ASTM International, West Conshohocken, PA, 2005, www.astm.org.

48. ASTM E9-89a (2000), Standard test methods of compression testing of metallic materials at room temperature, ASTM International, West Conshohocken, PA, 2000, www.astm.org.

49. ASTM C1624-05(2010), Standard test method for adhesion strength and mechanical failure modes of ceramic coatings by quantitative single point scratch testing, ASTM International, West Conshohocken, PA, 2010, www.astm.org.

50. J. Y. Park, J. E. Davies, Red blood cell and platelet interactions with titanium implant surfaces, Clinical Oral Implants Research 11 (2000) 530–539.

51. B. D. Boyan, S. Lossdorfer, L. Wang, G. Zhao, C. H. Lohmann, D. L. Cochran, Z. Schwartz, Osteoblasts generate an osteogenic microenvironment when grown on surfaces with rough microtopographies, European Cells and Materials 6 (2003) 22–27.

52. F. Variola, J. Brunski, G. Orsini, P. T. de Oliveira, R. Wazen, A. Nanci, Nanoscale surface modifications of medically-relevant metals: state-of-the art and perspectives, Nanoscale 3 (2011) 335–353. DOI: 10.1039/c0nr00485e

53. L. Facchini, E. Magalini, P. Robotti, A. Molinari, S. Höges, K. Wissenbach, Ductility of a Ti–6Al–4V alloy produced by selective laser melting of pre-alloyed powders, Rapid Prototyping Journal 16 (2010) 450–459. DOI: 10.1108/13552541011083371

54. B. Vrancken, L. Thijs, J. P. Kruth, J. Van Humbeeck, Heat treatment of Ti6Al4V produced by Selective Laser Melting: Microstructure and mechanical properties, Journal of Alloys and Compounds 54 (2012) 177–185. DOI: 10.1016/j.jallcom.2012.07.022

55. J. R. Caeiro, P. González, D. Guede, Biomecánica y hueso (y II): Ensayos en los distintos niveles jerárquicos del hueso y técnicas alternativas para la determinación de la resistencia ósea, Revista de Osteoporosis y Metabolismo Mineral 5 (2013) 99–108. DOI: 10.4321/S1889-836X2013000200007

56. S. J. Bull, Failure mode maps in the thin scratch adhesion test, Tribology International 30 (1997) 491–498. DOI: 10.1016/S0301-679X(97)00012-1

57. S. Ferraris, A. Bobbiob, M. Miola, S. Sprianoa, Micro- and nano-textured, hydrophilic and bioactive titanium dental implants,-Surface & Coatings Technology 276 (2015) 374-383. DOI: 10.1016/j.surfcoat.2015.06.042

Figure captions.

Figure 1. SEM images of the surface of the five different Ti6Al4V samples, in which protuberances as a remnant of partially molten particles are observed.

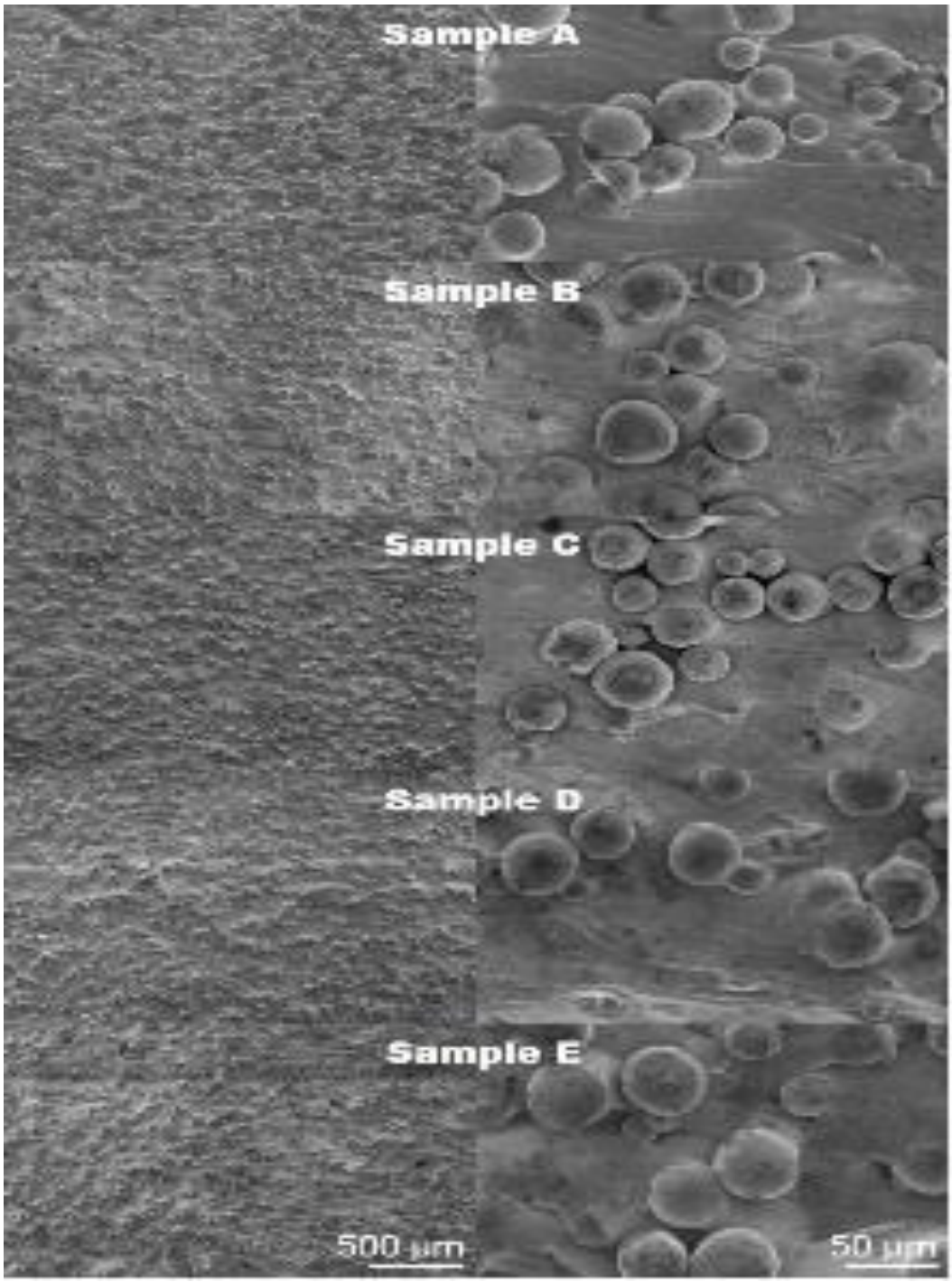

Figure 2. a) Particle size of the raw material (RM) and b) protuberance sizes on the studied surfaces (A, B, C, D and E).

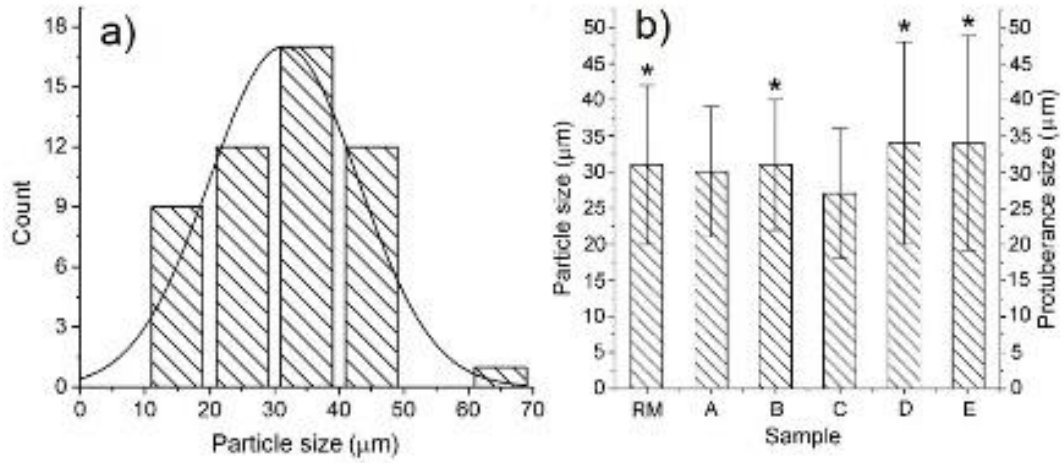

Figure 3. Details of the surface in samples D and E, in which cracked protuberances and the support beneath the attacked surface are observed.

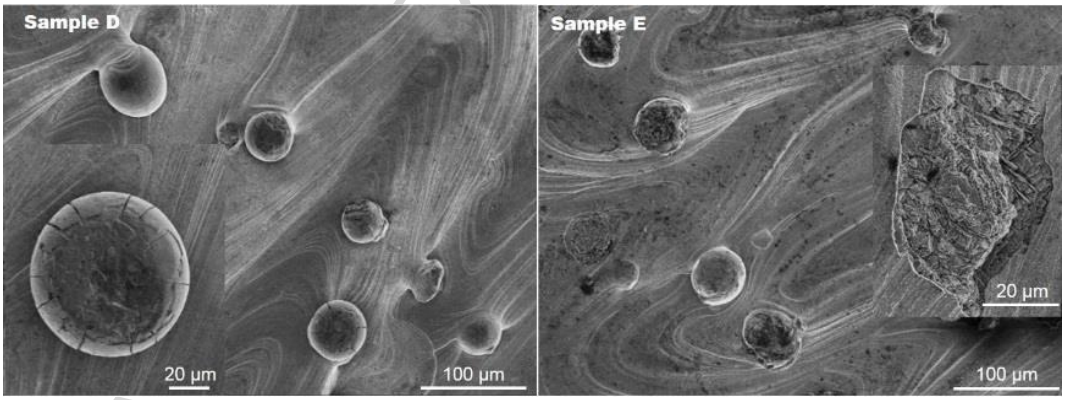

Figure 4. High-magnification micrographs of the surface of the five different Ti6Al4V samples, in which, except for sample A, the presence of an oxide layer was observed.

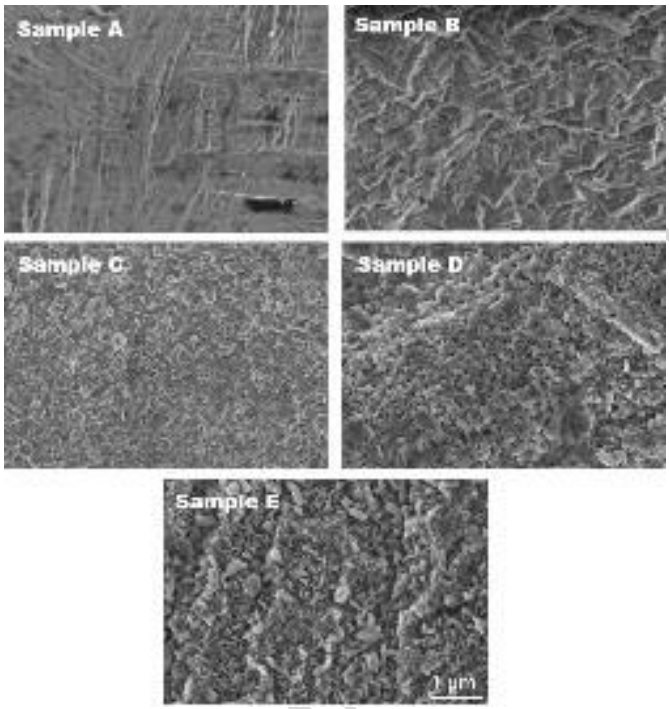

Figure 5. XRD patterns performed on the surface of Ti6Al4V samples.

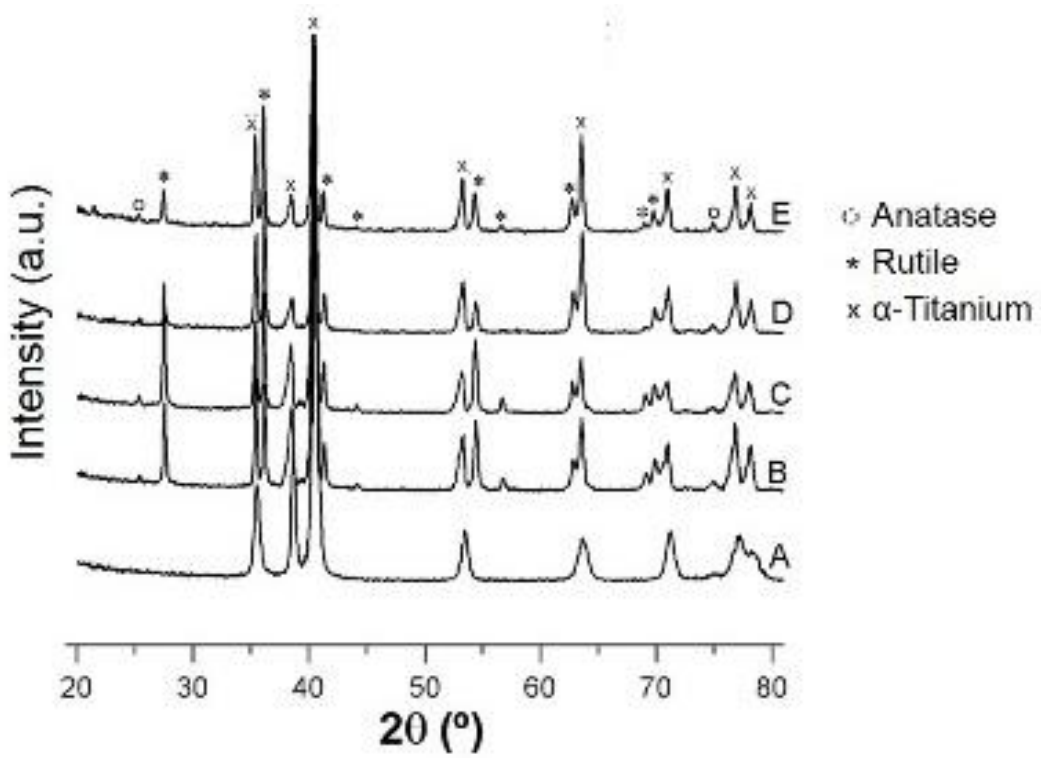

Figure 6. XEDS-SEM spectra of the surface of Ti6Al4V samples A and D. The presence of oxygen is clearly observed in sample D.

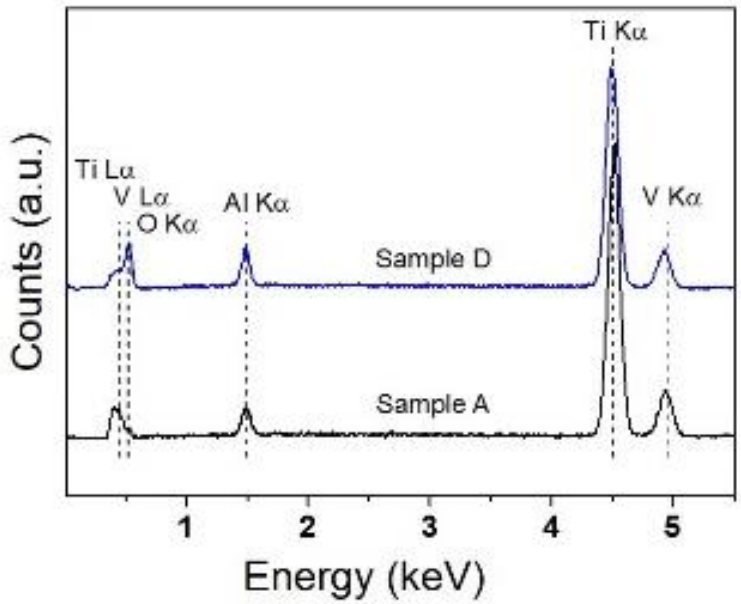

Figure 7. Surface roughness profile of Ti6Al4V samples.

Figure 8. Elastic recovery of Ti6Al4V samples during scratch test (load 20 N). Difference between the in-situ penetration depth (blue curves) and the real plastic deformation associated with the scratch tests (red curves). A) Bulk, b) Sample A, c) Sample B, d) Sample C, e) Sample D, f) Sample E.

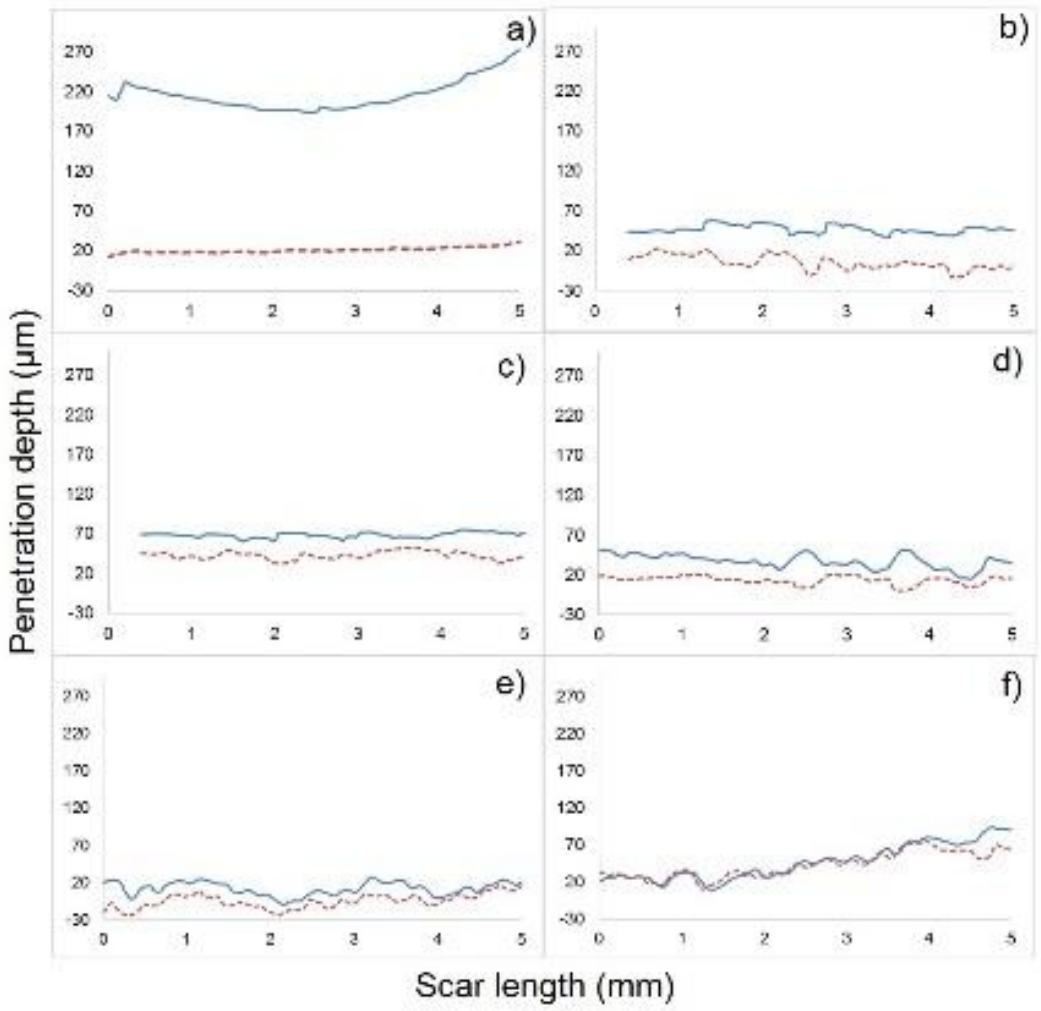

Figure 9. SEM images of micro-scratch scars on the surface of Ti6Al4V samples.

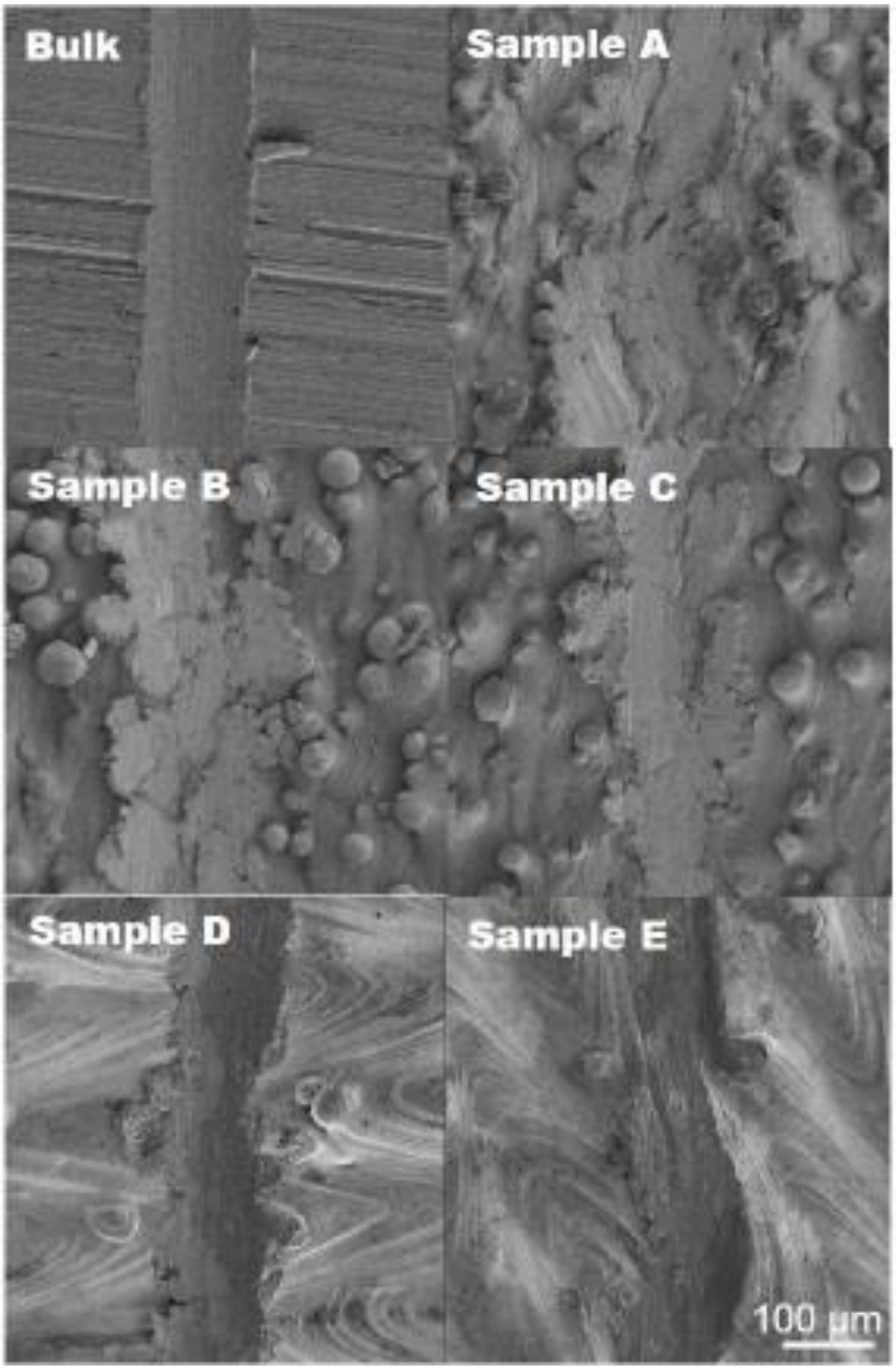

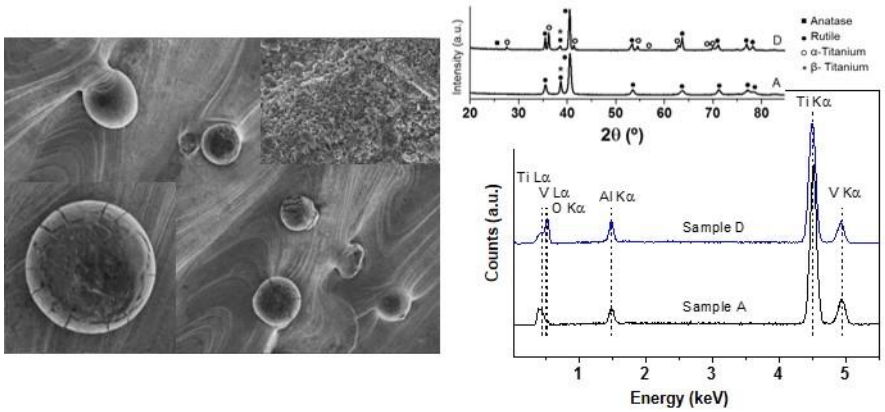

Graphical abstract

Surface modification of Ti-6Al-4V alloys manufactured by selective laser melting: Microstructural and tribo-mechanical characterization

Y. Torres et al.

Highlights.

- Ti-samples sintered by SLM with surface treatment to improve osseointegration.
- Formation of Ti-oxide layer which enhances bioactivity of the surface
- Micro-tribomechanical behavior is evaluated.